Ultrasonics 97 (2019) 38–45

Contents lists available at ScienceDirect

Ultrasonics

journal homepage: www.elsevier.com/locate/ultras

# Ultrasound focuser: A multi-cylindrical source configuration and entrapped particles dynamics

Majid Rajabi[a,*], Alireza Mojahed[b], Aria Hajiahmadi[a]

[a] Sustainable Manufacturing Systems Research Laboratory, School of Mechanical Engineering, Iran University of Science and Technology, Narmak, Tehran, Iran
[b] Linear and Nonlinear Dynamics and Vibrations Laboratory, Department of Mechanical Science and Engineering, University of Illinois at Urbana-Champaign, Urbana, IL 61801-2307, USA

ARTICLE INFO

*Keywords:*
Acoustic trapping
Acoustic focusers
Advanced delivery systems
Acoustic active carriers
Acoustic driven virtual channels

ABSTRACT

We aim to introduce the proof of concept of a 3D ultrasound Focuser with possible advanced applications in living-matter/cell entrapment, particle focusing, transportation through virtual channel and drug, agent or material delivery systems. The proposed mechanism is assumed to be fully submerged in a fluidic environment and composed of three parallel acoustic line sources which are located in such a way that form a triangular right prism. By approximating the wave field of each cylindrical source as a progressive plane wave field whose amplitude decreases with respect to the travelling distance from the source, the acoustic radiation force exerted on a single particle is analytically derived. It is shown that when each source has a $\pi/3$ phase different from other sources, an attracting zone around the axis of the triangular prism is formed for wavelengths in the order of the size scale, $\lambda/l \sim O(1)$, where $l$ denotes the distance between each two sources. The optimal operating situation (the largest attracting zone) is found for the case where $\lambda \approx l$. The theoretical study is supported by stability analysis of dynamics of the entrapped particle which located on the axis of the prism; and validated by computing the trajectories of migration of the test particle. The stability analysis is performed by considering the unsteady solution of Stokes equations and the possible flow of environmental fluid medium. In addition, the required settling time and required length scales to focus the particle to the center line of the prism for different size scale ratios are estimated and discussed. Compared to other 3D focusing techniques, this method is non-invasive, robust, easy to implement, applicable to nearly all types of micro-particles and does not need any specific pre-designed channel for focusing process.

## 1. Introduction

In the revolutionary race towards miniaturization, the advent of mili-, μm- and molecular sized machines and mechanisms, may expedite the evolution and progress in modern medicine, biomicrofluidics, biotechnologies and biomedicine. Considering the particle/cell/agents/drugs delivery and entrapment as a vital facility in various applications in microfluidic lab-on-chips, biochemistry and biomedical imaging [1], cell separation application [2], nanotechnology [3], drug delivery [4], gene therapy [5], genomic DNA [6–8], etc. [9–14], the importance of focusing, trapping and manipulation mechanisms are cleared. In the aforementioned applications, utilizing force, wave or flow fields (e.g., acoustical [15–28], optical [29–31], electro-kinetic [32,33] and hydrodynamics [34–37]) are typical and vastly employed.

The techniques based on the acoustics, have some merits compared to others due to its non-invasive nature, in-depth penetration, the sufficient amplitude of driving force, relatively low settling-time, etc. The common methodologies are based on pushing the object toward the target area by acoustic tweezers [38–47] and localizing it using standing wave fields produced by counter-side transducers or possible wave reflectors [16,20,48–50], two-crossed plane waves approach [51], single focused acoustic beam manipulators [41,43,45,52–56] and the standing surface acoustic waves (SSAW) produced by interdigital transducers [28].

In the present work, we propose a design for a small device which may serve as a focuser, trapper and virtual transportation channel, composed of three parallel ultrasonic line sources located in such a way whose top view depicts an equilateral triangle, which radiate in their breathing mode (monopole vibration), monochromatically but with adjusted phase difference. Considering the analytical solution for the acoustic radiation force exerted on a particle with relatively smaller size in comparison with the size of the prism, it is shown that the subsequent

* Corresponding author.
*E-mail address:* majid_rajabi@iust.ac.ir (M. Rajabi).

https://doi.org/10.1016/j.ultras.2019.04.007
Received 11 December 2018; Received in revised form 17 April 2019; Accepted 30 April 2019
Available online 30 April 2019
0041-624X/ 

phase differences of $\pi/3$ between sources leads to formation of a pressure nodal line on the axis of the prism which induces an area of attraction for wavelength-to-prism-length ratio of order of unity.

Considering the possible applications of the proposed configuration as a trapper, the performance of trapping is evaluated by solving the Stokes equations in order to estimate the trajectories of assumed particle initially located at different positions, e.g. within and outside the attracting zone. In order to check the performance of the proposed configuration as a focuser or as a guiding channel, it is assumed that the particle has pre-determined motion along the axis of prism due to the environmental fluid flow. The trajectories of particle are obtained and the quality of approach toward the axis of the prism is discussed. Moreover, the required settling-time and the required axial distance along the prism are obtained and the geometrical practicability is discussed.

The authors are confident that the proposed configuration can serve as a simple and practical idea of adaptive and flexible focuser or trapper or transportation channel, since its size can vary by a simple telescopic mechanism and its frequency of operation is not limited to a specific value due to its general piezoelectric based transducer and may be adapted to the required size of operation. Moreover, as a focuser, there is no need for a channel and the device is able to operate within an unbounded fluidic medium or may be used as a sampler in bio-fluidic environments. In addition, the focusing/trapping volume is efficient with respect to the total occupied volume of device. Generally, the introduced configuration can be an alternative asset of the other techniques and solutions given in the literature, with its special advantages and possible challenges.

## 2. Formulation

Fig. 1 shows the general geometry of the trapper with the shape of prism, which its face is an equilateral triangle. The side length of the triangle is denoted by $l$. It is assumed that the height of the prism is sufficiently larger than the triangle length scale, so that the dynamics of the problem could be regarded as 2D (two dimensional) problem. The line sources of acoustic field are located at the corner lines of the prism, radiating ultrasonic waves monochromatically with frequency of $\omega$.

In order to examine the functionality of the proposed mechanism in creating an attraction zone for drug or material entrapment, a test particle with spherical geometry is chosen. The radius of particle is denoted by $a$, assuming $a << l$. For simplicity, the particle is assumed to be non-deformable and neutrally buoyant.

Distances of the particle from each source and the corresponding angles are denoted by $(d_1, \alpha_1)$, $(d_2, \alpha_2)$ and $(d_3, \alpha_3)$, respectively. Additionally, Fig. 1 depicts the spherical particle which is insonified by three incident waves from each source. With the limitation of $a/\lambda << 1$ where $\lambda$ denotes the wavelength of the incident waves, the incident waves from each source in any relative angles and distances of the particle from the sources is assumed to be Pseudo-plane wave with its amplitude decreasing relation with the distance, $\propto d_j^{-1/2}$ (See Appendix A). The justification for the mentioned approximation and its negligible effect on the radiation force estimation is discussed in numerical results and analysis section.

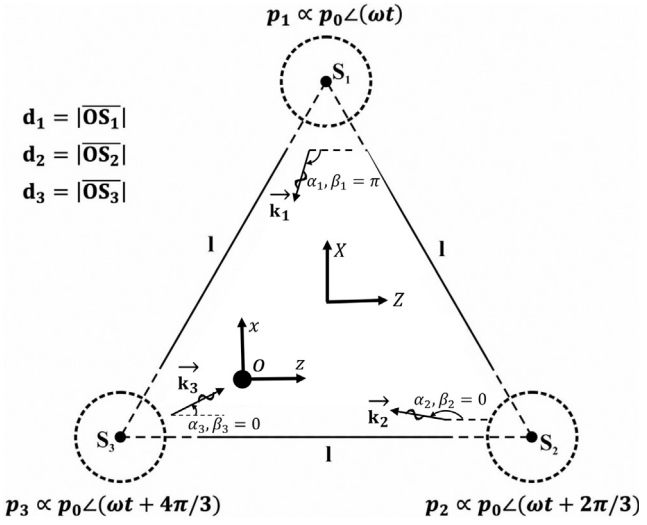


**Fig. 1.** Configuration of the problem.

A challenge in practice which may question the viability of the model, is the coupling mechanism which connects the transducers and its effects on the acoustic field due to possible end-effect. Considering telescopic slender rod connections between the transducers just at the top and the bottom of the configuration, the assumed free unbounded fluidic medium condition seems reasonable and the effects of the assumed connecting links between the transducers may be limited. In other words, away from the top and bottom boundaries the end-effects are rendered negligible, thus not drastically affecting the predicted results.

### 2.1. Acoustic field equations

Following the standard methods of theoretical acoustics, governing equations for an inviscid and ideal compressible fluid medium that cannot support shear stresses may be expressed respectively as [57]

$$\frac{\partial \rho}{\partial t} + \nabla.(\rho \mathbf{v}) = 0, \tag{1}$$

$$\rho\left(\frac{\partial \mathbf{v}}{\partial t} + \mathbf{v}.\nabla \mathbf{v}\right) + \nabla p = 0. \tag{2}$$

where $\rho$ is the fluid density, $\mathbf{v}$ is the fluid particles' velocity and $p$ denotes the ambient pressure. In linear acoustic, the above equations are simplified to

$$\frac{\partial \rho}{\partial t} + \rho_f \nabla.\mathbf{v} = 0. \tag{3}$$

$$\rho \frac{\partial \mathbf{v}}{\partial t} + \nabla p = 0. \tag{4}$$

where $\rho_f$ denoted the density of fluid host medium in equilibrium state. Combination of Eqs. (3) and (4) leads to

$$\frac{\partial^2 \mathbf{v}}{\partial t^2} = c^2 \nabla(\nabla.\mathbf{v}), \tag{5}$$

where $c = \{(\partial p/\partial \rho)_s\}^{1/2}$ is the speed of sound in fluid host medium, and where subscript "*s, 0*" means the constant entropy. Assuming the irrotational nature of the wave propagation phenomenon, the velocity vector can be expressed as a gradient of a scalar potential function, $\mathbf{v} = -\nabla\psi$. Substitution of this expression into Eq. (3) yields to

$$\frac{\partial^2 \psi}{\partial t^2} = c^2 \nabla^2 \psi. \tag{6}$$

Considering the monochromatic nature of the wave fields, oscillating with the frequency of $\omega$, the feasible description of the form $\psi(\mathbf{r}, t) = Re(\varphi(\mathbf{r})\, e^{-i\omega t})$ leads to the so-called Helmholtz equation as [57]

$$(\nabla^2 + k^2)\varphi = 0, \tag{7}$$

where $k = \omega/c$ is the wave number for the dilatational wave. The solution of the above equation according to the boundary conditions of the system leads to evaluation of the velocity vector field by $\mathbf{v} = -\nabla\psi(\mathbf{r}, t)$ and the acoustic pressure via $p(r, \theta, \omega) = \rho\, \partial\psi(\mathbf{r}, t)/\partial t$.

It can be shown that the expansions of the scalar velocity potential function of inclined incident plane wave satisfying Eq. (5), have the form of below [57]

$$\varphi_{rad.}(r,\theta,\omega) = 4\pi\varphi_0 s \sum_{j=1}^{3}\sqrt{\frac{2\pi}{k^3 d_j}}\sum_{n=0}^{\infty}\sum_{m=-n}^{m=n} j_n(kr)\,\bar{Y}_n^m(\alpha_j,\beta_j)\,Y_n^m(\theta,\varphi)\, e^{i[kd_j+\xi_j-(2n+1)\pi/4]}, \tag{8}$$

where $j_n$ is the spherical Bessel function of the first kind of order $n$, $Y_n^m = \sqrt{(2n+1)(n-m)!/[4\pi(n+m)!]}\,P_n^m(\cos\theta)e^{im\varphi}$ are spherical harmonics, $P_n^m$ are associated Legendre polynomials and the over-bar denotes the complex conjugate of the respective function [58], $\xi_j$, $j = 1, 2, 3$ is the phase index associated with the sources. Also, $(d_j, \alpha_j, \beta_j)$ denotes the distance of the particle from each source and the corresponding polar and azimuthal angle of the incident wave interacting with the particle. Notice that the harmonic time variations throughout the manuscript with $e^{-i\omega t}$ dependence, suppressed for simplicity. $|p_{rad.,0}| \sim O(\varphi_0\rho\omega)$ is the order of amplitude of the radiating acoustic pressure at the vicinity of sources. Eq. (8) can be rewritten as (See Appendix A)

$$\varphi_{rad.}(r,\theta,\omega) = \varphi_0\sum_{n=0}^{\infty}\sum_{m=-n}^{m=n} I_n^m j_n(kr)\,Y_n^m(\theta,\varphi), \tag{9}$$

where

$$I_n^m = 4\sqrt{2}\,\pi s\,[\bar{Y}_n^m(\alpha_1,\pi)e^{i[kd_1+\xi_1-(2n+1)\pi/4]}/(\sqrt{k^3 d_1}) + \bar{Y}_n^m(\alpha_2,0)e^{i[kd_2+\xi_2-(2n+1)\pi/4]}/(\sqrt{k^3 d_2}) + \bar{Y}_n^m(\alpha_3,0)e^{i[kd_3+\xi_3-(2n+1)\pi/4]}/(\sqrt{k^3 d_3})].$$

Likewise, the scattered wave field can be written as [57]

$$\varphi_{sc.}(r,\theta,\omega) = \varphi_0\sum_{n=0}^{\infty}\sum_{m=-n}^{m=n} A_n^m h_n(kr)\,Y_n^m(\theta,\varphi), \tag{10}$$

where $A_n^m = a_n^m I_n^m$, $h_n(x) = j_n(x) + iy_n(x)$ is the spherical Hankel function of the first kind of order $n$ [58], $A_n^m$ which is the unknown modal scattering coefficient determined by employing the appropriate boundary conditions, later. Considering the superposition principle in linear acoustic regimes, the total velocity potential, the velocity field and the acoustic pressure in surrounding medium can be evaluated by

$$\varphi_{t.} = \varphi_{sc.} + \varphi_{rad.},$$

$$v = -\nabla(\varphi_{sc.} + \varphi_{rad.}),$$

$$p_{t.} = p_{sc.} + p_{rad.} = -i\omega\rho(\varphi_{sc.} + \varphi_{rad.}). \tag{11}$$

Assuming the particle as an ideal rigid sphere, the boundary condition on the surface of the particle can be written as

$$\partial\varphi_{t.}(r,\theta,\omega)/\partial r|_{r=a} = 0. \tag{12}$$

Substituting Eqs. (9) and (10) into (11) and then into (12), yields $a_n^m = -j_n'(ka)/h_n'(ka)$.

### 2.2. Acoustic radiation force

In nonlinear acoustic regime, a body insonified by a sound field is known to experience a time-averaged force that is called the acoustic radiation force. For the case of a time-harmonic wave field, the time averaged radiation force can be written as

$$\langle\mathbf{F}\rangle = -\iint_S [((\rho/2c^2)\langle(\partial\psi_{t.}/\partial t)^2\rangle - (\rho/2)\langle|\nabla_\alpha\psi_{t.}|^2\rangle)\mathbf{n} + \rho\langle(v_n\mathbf{n} + v_t\mathbf{t})v_n\rangle]\,dS$$

where $\langle(.)\rangle = (\omega/2\pi)\int_0^{2\pi/\omega}(.)\,dt$ is the time average operator, $\psi_{t.} = \psi_{rad.} + \psi_{sc.}$ is the real part of the total potential function in host medium, $v_n = -\partial\psi_{t.}/\partial r$ and $v_t = -\partial\psi_{t.}/r\partial\theta$ are the radial and tangential components of velocity vector, $\mathbf{v} = -\nabla\psi_{t.}(\mathbf{r}, t)$. Substitution of Eqs. (5) and (6) into above expression of radiation force and using far-field method to calculate the radiation force leads to [59]

$$\langle\mathbf{F}\rangle = E_{inc.}S_c(Y_x\mathbf{e_x} + Y_z\mathbf{e_z}), \tag{13}$$

where $E_{rad.} = \rho k^2\varphi_0^2/2$ is an indicator of incident wave energy density, $S_c = \pi a^2$ is the cross-sectional area of the spherical body, $Y_x$ and $Y_z$ are the components of dimensionless radiation force function, $Y = (Y_x^2 + Y_z^2)^{1/2}$, extracted as a function of the scattering coefficient, $A_n^m$, as

$$Y_x = \frac{1}{2\pi(ka)^2}\,\mathrm{Im}\sum_{n,m}(I_n^m + A_n^m)(A_{n+1}^{m-1*}b_{n+1}^{-m} + A_{n-1}^{m-1*}b_n^{m-1} - A_{n+1}^{m+1*}b_{n+1}^m - A_{n-1}^{m+1*}b_n^{-m-1}),$$

$$Y_z = \frac{1}{(ka)^2}\,\mathrm{Im}\sum_{n,m}(I_n^m + A_n^m)(A_{n+1}^{m*}c_{n+1}^m - A_{n-1}^{m*}c_n^m). \tag{14}$$

where $b_n^m = \{[(n+m)(n+m+1)]/[(2n-1)(2n+1)]\}^{1/2}$ and $c_n^m = \{[(n-m)(n+m)]/[(2n-1)(2n+1)]\}^{1/2}$.

### 2.3. Particle dynamics

The equation of motion of a small spherical particle moving within a viscous fluid can be written as [60]

$$m_p\frac{dv_i}{dt} = -6\pi\eta a v_i - \frac{1}{2}m_f\frac{dv_i}{dt} - 6\pi\eta a^2\int_0^t d\tau\frac{dv_i/d\tau}{[\pi\nu(t-\tau)]^{1/2}} + F_i, \tag{15}$$

where $v_i$ is the velocity of the particle, $m_p \cong (4/3)\pi a^3\rho$ is the mass of particle. The first term in the right-hand side of Eq. (15) is known as the "Stokes drag", in which $\eta$ is the dynamic viscosity of the fluid, and $a$ is the particle radius, next two terms are the added-mass-force and history-force, respectively. Moreover, $m_f \cong (4/3)\pi a^3\rho$ is the mass of displaced fluid, and $\nu = \eta/\rho$ is the kinematic viscosity of the fluid. These three forces represent the unsteady forces acting on the particle [61,62]. Lastly, the final term, $F_i$, is the external force acting on the particle which for our case denotes only the acoustic radiation force.

A Laplace transform applied to Eq. (15) for a test particle which starts at rest, leads to

$$[(m_p + m_f/2)s + 6\pi\eta a + (6\pi\eta a^2/\nu^{1/2})s^{1/2}]\hat{v}_i = \hat{F}_i, \tag{16}$$

where $\wedge$, represents variables in the Laplace domain, and $s$ is the Laplace variable.

The temporal evolution of particle velocity is calculated using the convolution $v_i = f * g = \int_0^t F_i(t-\tau)g(\tau)d\tau$ where $g$ is $g = L^{-1}\{1/[(m_p + m_f/2)s + 6\pi\eta a + (6\pi\eta a^2/\nu^{1/2})s^{1/2}]\}$ and $L^{-1}\{.\}$ denotes the inverse-Laplace operator.

Considering the Cartesian coordinate system in Fig. 1 and the component of acoustic radiation force as $F_x = E_{inc.}S_cY_x$, $F_z = E_{inc.}S_cY_z$ and $F_y = 0$, the particle temporal velocity components can be computed numerically by the aforementioned convolution integral. Obviously, for the velocity component of particle along the $Y$-axis (i.e., the axis of prism) in the existence of axial background flow of environmental fluid medium, $v_y$ is obtained as $v_y = v_{y,0}$ in which the subscript "$y$, 0" denotes the value of $v_y$ at $t = 0$, which is describes the background flow-field velocity. The trajectory of migration then can be calculated by numerical integration of velocity components. In the limiting case of steady-state, the velocity field can be analytically determined as $v_x = F_x/(6\pi\eta a)$, $v_z = F_z/(6\pi\eta a)$ and $v_y = v_{y,0}$ and the trajectory of the particle can be approximated as $dX/dZ = -v_x/v_z = -Y_x/Y_z$, $Y = v_{y,0}\,t + Y_0$.

## 3. Numerical results and analysis

### 3.1. Acoustic pressure and radiation force distribution

The proposed idea of making an attractive zone within the trapper is to form a pressure node at the geometrical center of the trapper, i.e. axis of the prism, by adjusting $\xi_1 = \xi_2 + 2\pi/3 = \xi_3 + 4\pi/3$. In order to examine the feasibility of the proposed mechanism, several numerical examples are considered. The host medium characteristics are assumed

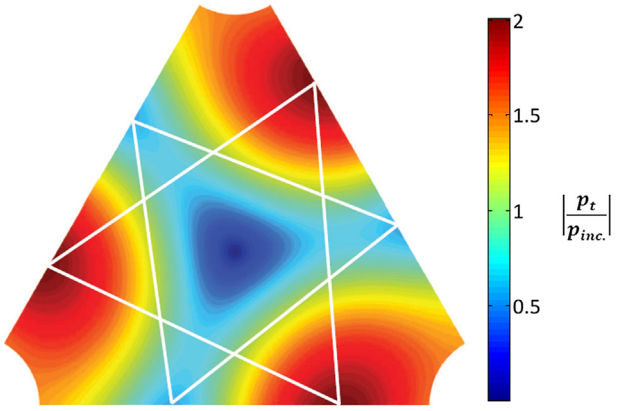


**Fig. 2.** 2D contour plot pattern of normalized pressure amplitude inside the trapper.

to be $\rho = 1000\,\mathrm{kg/m^3}$ ($\sim O(10^3)\,\mathrm{kg/m^3}$) and $c = 1400\,\mathrm{m/s}$ ($\sim O(10^3)\,\mathrm{m/s}$) and the radiating pressure-amplitude, $|p_{rad.}|$, is set to be of order $\sim O(10^4)\,\mathrm{Pa}$. After numerous simulations with the qualitative objective function of making the maximum area of attraction, the optimal order of wavelength of the sources is found as $\lambda/l \sim O(1)$. Several sizes of the trapper are considered as $l = \lambda = 10^2, 10^3, 10^4\,\mu\mathrm{m}$ which indicate $kl = 2\pi$. For each selected size of the trapper, the test particle size is assumed to be in range of $0.01 < a/l < 0.1$. The lower limit of the particle size is due to this fact that for small size of particles, the magnitude of the induced acoustic force is so small that the convergence and settle down of particles is too time consuming and the process is not efficient. Also, for very small particles, other forces such as surface tractions become comparable to the generated radiation force acting in the particle. The operating frequencies of interest are considered to be $f = \omega/2\pi = c/\lambda = 1.4 \times 10^7,\ 1.4 \times 10^6,\ 1.4 \times 10^5\,\mathrm{Hz}$, respectively. The required frequencies of operation belong to the range of $\sim O(10^2)\,\mathrm{kHz} - \sim O(10^1)\,\mathrm{MHz}$ which is practical and feasible.

Fig. 2 illustrates the 2D contour plot pattern of normalized pressure amplitude, $p_t/p_{rad.,0}$, inside the trapper. All the size scales are normalized. The required pressure node at the center of the trapper is formed and three anti-nodes are generated on the virtual sides of the trapper. Also, a low pressure region around the central node is seen which is similar to a triangle which we will refer to as "*attraction triangle*" from this point on. The white lines connect the three pressure nodes and the three pressure anti-nodes, which are located such that two virtual triangular patterns are formed.

Fig. 3 depicts the 2D contour plot of the amplitude of dimensionless radiation force function, $|Y = Y_x\hat{\boldsymbol{e}}_x + Y_z\hat{\boldsymbol{e}}_z|$, for the test particle with size ratio of $a/l = 0.05$, which at selected points, its direction is demonstrated with arrows (i.e., the length of arrows is linearly proportional to

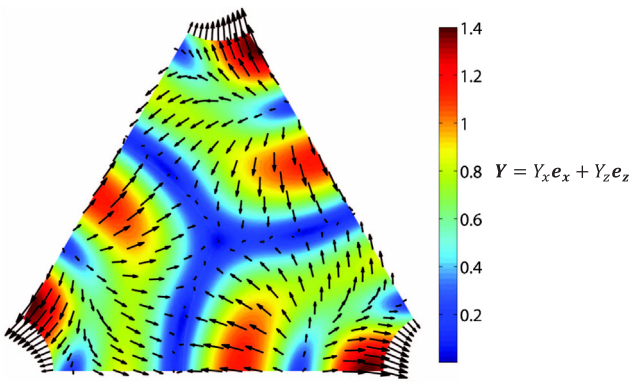


**Fig. 3.** 2D contour plot of the amplitude of dimensionless radiation force function and its direction, which is shown as an arrow.

the amplitude of the force). To relate Figs. 2 and 3 one can clearly observe that the radiation force on the pressure antidotes on the sides of the triangle, illustrate local minima. Moreover, an interesting twisted Star-like pattern is observed in which minimum zones of radiation force occur. The (three) minimums of the radiation force occur on the wings of the star-like region which are consistent with the corners of the *attraction triangle*. It should be noted that for other sizes of test particle, the general pattern of the normalized radiation force is similar to that shown in Fig. 3, but with different amplitudes which may be approximated as $|Y| \propto a$.

Considering the challenge of acoustic streaming, following the estimation of Doinikov [63–67] for acoustic viscous boundary layer thickness, $\delta$, as $\sim O([\eta/(\rho\omega)]^{1/2}) \sim O(10^{-1})\,\mu\mathrm{m}$, and considering the situation of $\delta < a < l$, one can disregard the effects of acoustic streaming while not introducing large errors in the analysis with the same assumptions as presented paper [47].

In order to justify approximating cylindrical wave field with pseudo-plane wave field, we should ensure that the estimated radiation force does not deviate from the true radiation force generated by cylindrical sources, in our case of study. Looking at Hasegawa et al. 1981 [68] in which the radiation force is obtained for a solid sphere subjected to spherical (curved) wave field, it is found that for $ka < 1$ where $k = 2\pi/\lambda$ is the wave number of incident wave, the radiation force associated with a curved wave front of incident acoustic field is similar to the radiation force acting on a sphere located at infinity where the wave front resembles a plane wave, independent of the material properties of sphere and the distance ratio, $d/a$.

### 3.2. Stability analysis of particle dynamics at center-line

Considering the centerline (axis) of the prism as the a fixed-points of the entrapped/focused particle, the stability of this fixed-point can be determined via examining the eigenvalues of the variational matrix of the corresponding in xz-plane as

$$J^* = \begin{bmatrix} [0]_{2\times2} & [I]_{2\times2} \\ (1/\alpha)[\partial F_i/\partial r_j]_{2\times2} & \begin{bmatrix} -6\pi\eta a/\alpha & 0 \\ 0 & -6\pi\eta a/\alpha \end{bmatrix}_{2\times2} \end{bmatrix}, \tag{17}$$

where $[I]_{2\times2}$ is the identity matrix, $[\partial F_i/\partial r_j] = \begin{bmatrix} \partial F_x/\partial X & \partial F_x/\partial Z \\ \partial F_z/\partial X & \partial F_z/\partial Z \end{bmatrix}$, and $\alpha = m_p + m_f/2$. The above Jacobian (variational) matrix is obtained by linearization of the equations of motion around the center line, ignoring the effects of history force. For our case of study, the eigenvalues take the form of $\gamma_i = \alpha_i(\omega) \pm j\beta_i(\omega),\ i = 1, 2$ in which the negative values of $\alpha_i(\omega)$ means stability and the positive values indicate that the fixed-point in xz-plane is unstable.

For the case of $l = 100\,\mu\mathrm{m}$, $a = 5\,\mu\mathrm{m}$ and $ka \approx 0.314$, we found $\gamma_1 = -1.0080 \pm 0.4053j$ and $\gamma_2 = -1.068 \times 10^5 \pm 0.4053j$ which denotes stability with possible oscillatory behavior. The stability analysis is done for the range of particle size, $0.01 < a/l < 0.1$. Fig. 4(a)–(d) show the variation of $\alpha_1, \beta_1, \alpha_2, \beta_2$ as functions of $a/l$, respectively. The locus of stable equilibrium points is found to be a spiral curve for the mentioned size ratio, which it is expected that the entrapped particles size scales perform inward spiral motion. The analysis is checked for other size scales of $l = 1000\,\mu\mathrm{m}$ and $l = 10,000\,\mu\mathrm{m}$, and the same conclusion is drawn.

### 3.3. Migration of particles – steady solution approximation

In order to visualize the performance of the suggested trapper/focuser, Fig. 5 illustrates the migration trajectories of the test particle, initiated form several different positions. The trajectories are plotted via the characteristic equation of $dZ/dX = -Y_z/Y_x$. This approximate relation is drawn from the low Stokes number condition and low Reynolds number approximation of Maxey and Riley governing equations

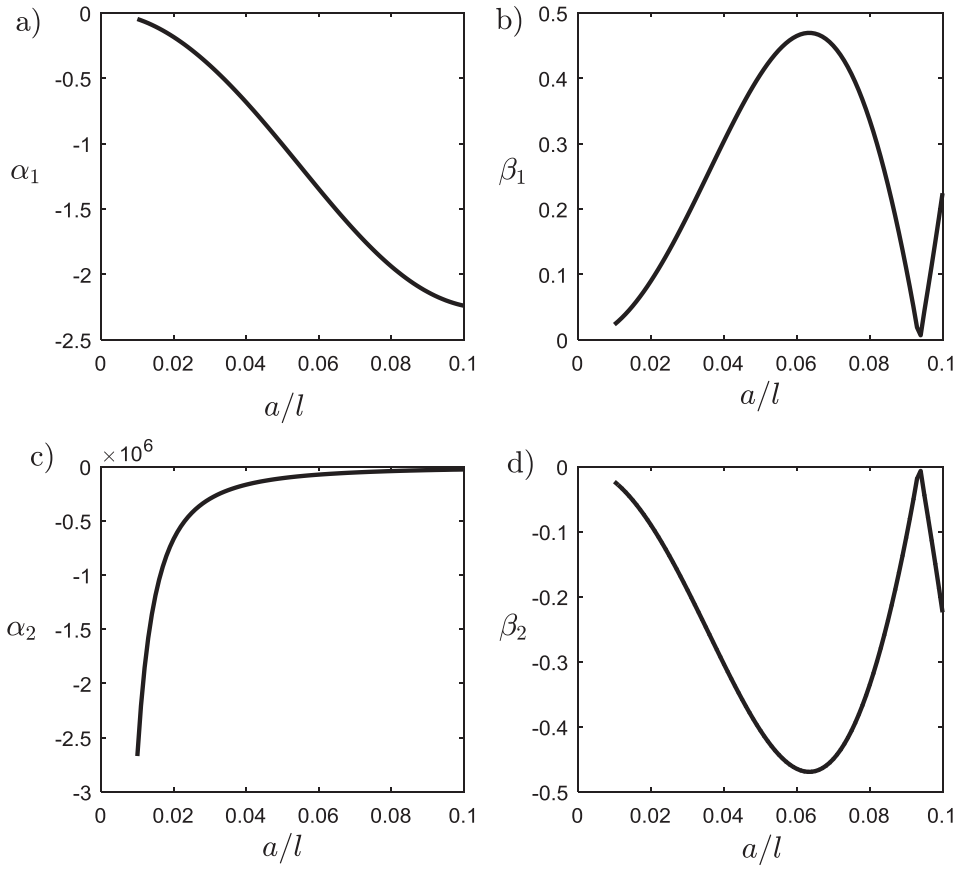


**Fig. 4.** The (a) real and (b) imaginary of first eigenvalue and the (c) real and (d) imaginary of the second eigenvalue corresponding to the Jacobian matrix for lateral stability (stability in xz-plane) analysis of central axis of trapper, as a function of size ratio, a/l.

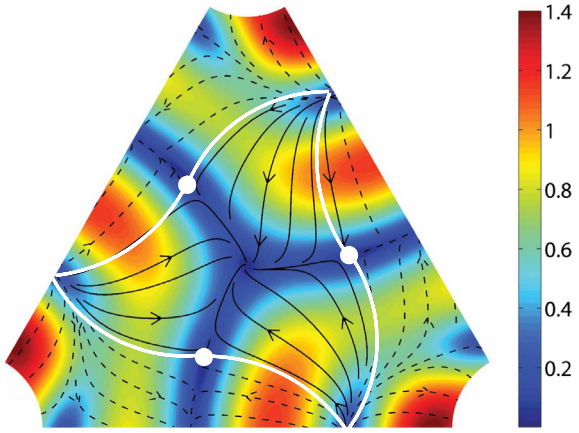

**Fig. 5.** Trajectories of the test particles, initiated form different positions in the trapper according to the steady dynamics approximated solution. Three nodes of radiation force inside the trapper are marked with white circles which may form a the circumscribed circle of the area of attraction, we may call basin of attraction, since all initial positions of test particles in this area leads to a trajectory inward the configuration, like an attractive basin. The trajectories are divides into attractive (i.e., continuous lines) and repulsive (i.e., dashed lines) types.

[60] which are condensed to the steady stokes theory [69–71]. For our study, the Stokes number as an index of characteristic time of a particle dynamics to the characteristic of flow dynamics which is defined as $Stk = t_0 v_s/a$, where $t_0$ is the relaxation time (i.e., the time constant in the exponential decay of the particle velocity due to the drag, which for our case of low Reynolds number condition and Stokes flow, may be approximated as $t_0 = 4\rho a^2/18\mu$), which is of order $\sim O(10^{-4})$, $\sim O(10^{-2})$ and $\sim O(1)$ for $l = 100\ \mu m$, $l = 1000\ \mu m$ and $l = 10,000\ \mu m$ respectively. It should be noted that as mentioned before, the size of test particle is in the range of $0.01 < a/l < 0.1$. In order to have steady solution approximation, all the unsteady inertial and history forces should be neglected and the only remaining force, i.e. the drag force, may be approximated as the well-known Stokes drag instead of Basset drag. Therefore, the external radiation force on the particle is balanced with the Stokes drag force as $<\mathbf{F}_d> = 6\pi\eta\, a\, \mathbf{v}_s$, where $\mathbf{v}_s$ is the particle velocity vector. Considering $<\mathbf{F}_d> \propto \mathbf{v}_s$, and quasi-stationary dynamics of trapped particle, the simplifications to obtain trajectories seems reasonable. The effects of unsteady terms on the dynamics and corresponding trajectories of test particle for various size scales are discussed later.

The trajectories are divided into attractive (i.e., continuous curves) and repulsive (i.e., dashed curves) types where for any initial position on the boundaries of attractive circle, the test particle moves inward within the trapper. As it is seen in Fig. 5, many of stable trajectories are initiated from the pressure antinodes on the sides of triangle. The stable trajectories approach (directly) towards the central node or (indirectly) the star-like wings and keep on migrating towards the center. The area of attraction may be distinguished by the condition of $\mathbf{Y}.\ \mathbf{e_r} \leqslant 0$, where $\mathbf{Y} = (Y_x \mathbf{e_x} + Y_z \mathbf{e_z})$ is the total radiation force function exerted on the test particle and $\mathbf{e}_r$ is the radial unit vector in *XY*-plane. The white curves in Fig. 5 show the boundaries of the area of attraction. As an indicator for the area of attraction, the diameter of its assumed circumscribed circle (i.e., illustrated by three white nodes in Fig. 5) is found as $d_s \sim 0.38\, l$.

Considering the area of *attraction circle* with respect to the prism area, it is concluded that approximately, half of the trapper can be regarded as the effective trapping volume for drug/material/agent or any

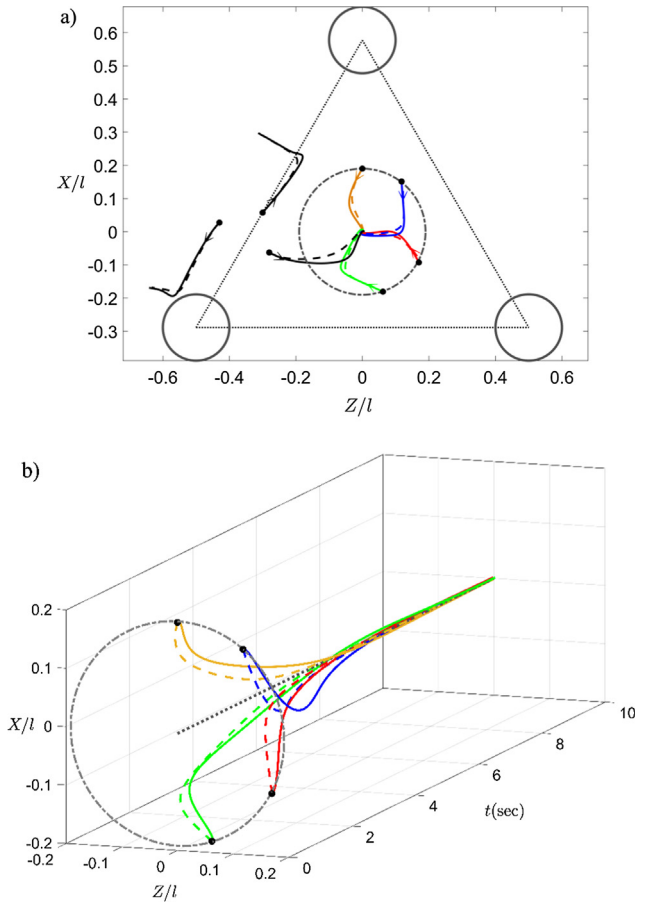


**Fig. 6.** (a) The planar (XZ-plane) trajectories of test particles, initially located at different positions but all of them are at rest state, for different size of trapper, but the same size ratio of $a/l = 0.05$, as: $l = 100\,\mu m$, $a = 5\,\mu m$, $l = 1000\,\mu m$, $a = 50\,\mu m$ and $l = 10,000\,\mu m$, $a = 500\,\mu m$. The initial positions of test particle are highlighted with black colored circles. The wave sources are schematically shown as circles. The trajectories corresponding to the cases of $l = 100\,\mu m$, $a = 5\,\mu m$, and $l = 1000\,\mu m$, $a = 50\,\mu m$, are coincident as well as the steady solution approximation which are shown with dashed lines. (b) The XZ-trajectories of test particles with respect to time, $0 < t < 10$ s.

other material which should be carried or cell/active matters/genes, etc., which should be captured in a biological system.

### 3.4. Migration of particles – unsteady solution and time of settle down

In this section, the effect of unsteady terms on the migration of test particles initially located at different positions for different size scales, are discussed. Moreover, an interesting quantity which may reflect the performance of the proposed configuration especially as a focuser in a transportation channel, is the time of settling down of the test particle along the central axis of prism and the corresponding trajectories.

Fig. 6(a) depicts the planar (*XZ*-plane) trajectories of test particles, initially located at different positions but all of them are at rest state, for different size of trapper, but the same size ratio of $a/l = 0.05$, as: $l = 100\,\mu m$, $a = 5\,\mu m$, $l = 1000\,\mu m$, $a = 50\,\mu m$ and $l = 10,000\,\mu m$, $a = 500\,\mu m$. Fig. 6(b) shows the *XZ*-trajectories with respect to time, $0 < t < 10$ s. In all cases, the wavelengths of the incident wave fields are kept $\lambda \approx l$. The initial positions of test particle are highlighted with black colored circles. The trajectories corresponding to the cases of $l = 100\,\mu m$, $a = 5\,\mu m$, and $l = 1000\,\mu m$, $a = 50\,\mu m$, coincide with the steady solution approximation which are shown with dashed lines. As the size of test particle increases to the last case of $a = 500\,\mu m$, even with the same size ratio, $a/l = 0.05$, the unsteady solution deviates from the steady one as it is shown with the continuous curves. This is due to the fact that for higher size of particle, the driving forces as well as the terms corresponding to the unsteady solution play the most influencing roles in the dynamics of the particle compared to the viscous terms. Also, it should be pointed out that the initial positions of the test particles are selected so that the functionality of the proposed device can be evaluated. Four initial positions on the attraction circle and three initial positions are selected close to one of the pressure anti-nodes on the side of the prism (See Fig. 2). As it was expected, all the initial positions on the boundary of attraction circle approach toward the center line of prism. Also, the initial position around the anti-node of pressure field which is inside the triangle is captured by the attracting basin, but the other trajectories are pushed outside the device due to the repulsive effect of anti-nodes of pressure.

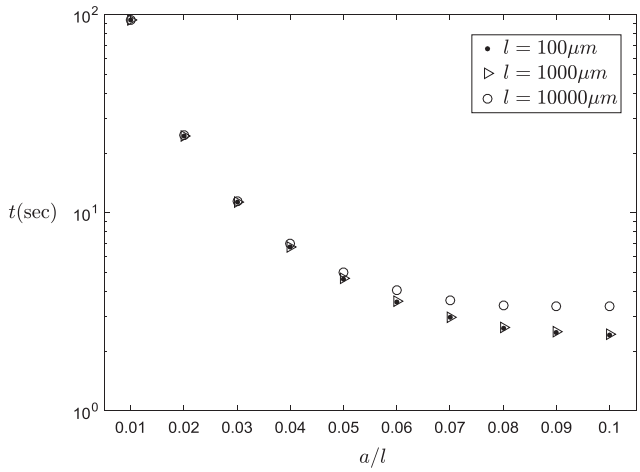


**Fig. 7.** The variation of maximum settling time for selected size ratios of test particle, $a/l = 0.01, 0.02, 0.03, 0.04, 0.05, 0.06, 0.07, 0.08, 0.09, 0.10$, for three cases of $l = 100\,\mu m$, $1000\,\mu m$, $10,000\,\mu m$.

In order to investigate the time of settling down, the criterion of $[X^2(t) + Z^2(t)]^{1/2} < 0.01\,d_s$ is assumed, in which $d_s$ is the diameter of the circumscribed circle of attraction area. Fig. 7 illustrate the variation of maximum time of settle down, for selected size ratios of test particle, $a/l = 0.01, 0.02, 0.03, 0.04, 0.05, 0.06, 0.07, 0.08, 0.09, 0.10$, and three cases of $l = 100\,\mu m$, $1000\,\mu m$, $10,000\,\mu m$. It is seen that the time of settling down is approximately equal for the two cases of $l = 100\,\mu m$, $1000\,\mu m$ for which similar trajectories were obtained from the steady solutions. For the case of $l = 10,000\,\mu m$, the time of settling down slightly deviates from the other two cases as $a/l$ increases and thus higher time of settle down is recorded. The difference is not considerable similar to the deviation between the trajectories. This implies that the same (slightly perturbed) dynamics governs the motion of the test particle where the perturbations originate from the unsteady effects associated with the history force, the added mass and the inertial effects. As it is observed, the time of settling down decreases as the size ratio of the test particle increases, from 93.90 s for $a/l = 0.01$, $l = 10,000\,\mu m$ and 93.85 s for $a/l = 0.01$, $l = 1000\,\mu m$ *and* $l = 100\,\mu m$ to 2.40 s for $a/l = 0.1$, $l = 100\,\mu m$, 2.43 s for $a/l = 0.1$, $l = 1000\,\mu m$ and 3.37 s for $a/l = 0.1$, $l = 10,000\,\mu m$. Considering an approximation for the time of migration as $t^* \propto l/v^* = \rho c^2\eta/[|P_{rad.}|^2 \bar{Y}\,(a/l)]$ in which $v^*$ indicates a characteristic averaged migration velocity scale, estimated as $v^* \propto \bar{F}/(6\pi\eta a) \propto [|P_{rad.}|^2/(\rho c^2\eta)](a/l)\,\bar{Y}$, where the over-bar denotes average over the path, it might be expected that for same size ratios, $(a/l)$, the same orders of time of migration is expected. Moreover, the viscosity of fluidic medium as well as the density and the sound speed (i.e., bulk modulus) have decelerating effects on the focusing/trapping process while the radiating acoustic pressure amplitude has accelerating effects.

Considering the proposed configuration as a focuser, the required length of settle down along the axis of prism is a key factor. In the used dynamic model, the motion of test particle is not influenced by the planar acoustic wave field along the *Y*-axis; therefore the governing equation of motion along the *Y*- axis leads to the simple solution of $Y(t) = v_{y,0}t$ where $v_{y,0}$ denotes the axial velocity of flow field associated with the fluidic host medium which assumed to be constant. For the small micron-scale case of $l = 100\,\mu$m, for particle size in the range of $0.01 < a/l < 0.1$, and practicable flow velocity of $v_{y,0} \sim O(10)\,\mu$m/s, the axial length for settle down is obtained in the range of $\sim O(0.1)l - \sim O(1)l$, which is suitable. For the relatively large scale case of $l = 10,000\,\mu$m, the same length scales for axial time of settle down is obtained for flow velocity of $v_{y,0} \sim O(10^3)\,\mu$m/s.

## 4. Conclusion

In the presented work, a new, simple and versatile mechanism composed of three parallel acoustic line sources for acoustic particle confinement purposes has been introduced. The proposed mechanism is composed of three parallel acoustic line sources which are located in such a way that form a triangular right prism. It is found that relatively large attractive region, compared to the volume occupied by the prism itself, is formed around the center line, i.e. axis, of the triangular prism for wavelengths within the order of size-scale of proposed configuration $\lambda/l \sim O(1)$, where $l$ denotes the length of triangle prism. The optimum operating condition (the maximum attractive zone) is found when $\lambda \approx l$. The study is supported by the linear stability analysis of the dynamics of entrapped test particle located on the center line, i.e. the trivial fixed point of the test particle, of the prism and the trajectories of migration and the required time/length for settling down, for several initial positions that are calculated by considering the unsteady solution of Stokes equations and the possible flow of environmental fluid medium. The authors hope that the proposed configuration may serve as a feasibility study of advanced assets for the applications of cell/living-matter trapper or drug/agent carrier or transportation channel or focuser.

## Appendix A. Pseudo-plane wave assumption of cylindrical wave field

Let a sphere of radius $a$ centered at point $O$ be excited by a line source at distance $d$ from point $O$ with an intensity of $s$. Consider the line source to be of infinite length parallel to y-axis (See Fig. A1).

According to [72], the incident wave generated by the line source can be written as

$$\varphi_{inc.} = \sum_{n=0}^{\infty}\sum_{m=0}^{n} A_n^m h_n(kr) P_n^m(\cos\theta) e^{im\phi}, \tag{A.1}$$

where $h_n(.)$ is spherical Hankel function of first kind and order $n$, $Y_n^m$ are the spherical harmonics and for the above relation to be valid, $\phi = 0,\ \pi$ should hold which exactly is the case in the presented paper. Also, $A_n^m$ are found to be [72]

$$A_n^m = -\frac{s}{k}\pi(2n+1)F(iH_j^{(2)}(kd),\, n,\, m), \tag{A.2}$$

in which $F$ is found by solving a system of $n$ equations given in Eq. (35) of [72] and $H_n^{(2)}(.)$ is the cylindrical Hankel function of second kind and order $n$.

In the presented paper, it is assumed that $ka$ is of order $O(10^{-1})$ and since it is assumed that the ratio $d/a$ is of order $O(10^1) - O(10^2)$, it can be acceptable to replace $H_n^{(2)}(kd)$ with its asymptotic formula up to order $O((kd)^{-1})$ as (The accuracy of this assumption discussed in Section 3.1)

$$H_n^{(2)}(kd) \approx \sqrt{\frac{2}{\pi kd}}\, e^{-i\left[kd-(2n+1)\frac{\pi}{4}\right]}, \tag{A.3}$$

which leads to

$$A_n^m = -s(2n+1)i\sqrt{\frac{2\pi}{k^3 d}}\, e^{-i\left[kd-(2n+1)\frac{\pi}{4}\right]}\delta_{m0}, \tag{A.4}$$

where $\delta_{ij} = \begin{cases} 1 & i = j \\ 0 & i \neq j \end{cases}$ is the kronecker delta function. Thus, the incident wave potential field can be rewritten as

$$\varphi_{inc.} = \varphi_0 s\sqrt{\frac{2\pi}{k^3 d}}\sum_{n=0}^{\infty}(2n+1)\, e^{-i\left[kd-(2n+1)\frac{\pi}{4}\right]} h_n(kr) P_n(\cos\theta). \tag{A.5}$$

Applying translational addition theorem to Eq. (A5), one can obtain Eq. (8) by considering three sources with phase difference.

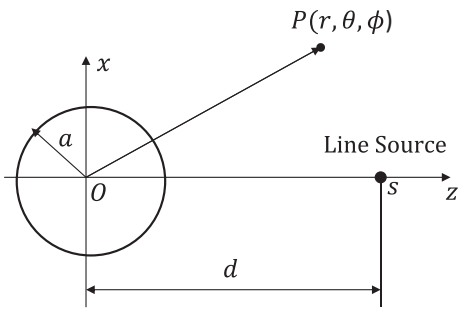


**Fig. A1.** Schematic of problem.

## References


[1] H. Masuhara, T. Asahi, Y. Hosokawa, Laser nanochemistry, in: Pure and Applied Chemistry, vol. 78, 2006, p. 2205.
[2] W.T. Coakley, Ultrasonic separations in analytical biotechnology, Trends Biotechnol. 15 (1997) 506–511.
[3] D.P. O'Neal, L.R. Hirsch, N.J. Halas, J.D. Payne, J.L. West, Photo-thermal tumor ablation in mice using near infrared-absorbing nanoparticles, Cancer Lett. 209 (2004) 171–176.
[4] D. Chatterjee, P. Jain, K. Sarkar, Ultrasound-mediated destruction of contrast microbubbles used for medical imaging and drug delivery, Phys. Fluids 17 (2005) 100603.
[5] Y.H. Lee, C.A. Peng, Enhanced retroviral gene delivery in ultrasonic standing wave fields, Gene Ther. 12 (2005) 625–633.
[6] U.F. Keyser, J.v.d. Does, C. Dekker, N.H. Dekker, Optical tweezers for force measurements on DNA in nanopores, Rev. Sci. Instrum. 77 (2006) 105105.
[7] U.F. Keyser, B.N. Koeleman, S. van Dorp, D. Krapf, R.M.M. Smeets, S.G. Lemay, et al., Direct force measurements on DNA in a solid-state nanopore, Nat. Phys. 2 (2006) 473–477.
[8] H. Oana, K. Kubo, K. Yoshikawa, H. Atomi, T. Imanaka, On-site manipulation of single whole-genome DNA molecules using optical tweezers, Appl. Phys. Lett. 85 (2004) 5090–5092.
[9] R. Gómez-Medina, P. San José, A. García-Martín, M. Lester, M. Nieto-Vesperinas, J.J. Sáenz, Resonant radiation pressure on neutral particles in a waveguide, Phys. Rev. Lett. 86 (2001) 4275–4277.
[10] H.M. Hertz, Standing-wave acoustic trap for nonintrusive positioning of microparticles, J. Appl. Phys. 78 (1995) 4845–4849.
[11] P.H. Jones, E. Stride, N. Saffari, Trapping and manipulation of microscopic bubbles with a scanning optical tweezer, Appl. Phys. Lett. 89 (2006) 081113.
[12] M.J. Marr-Lyon, D.B. Thiessen, P.L. Marston, Passive stabilization of capillary bridges in air with acoustic radiation pressure, Phys. Rev. Lett. 86 (2001) 2293–2296.
[13] P.L. Marston, D.B. Thiessen, Manipulation of fluid objects with acoustic radiation pressure, Ann. N. Y. Acad. Sci. 1027 (2004) 414–434.
[14] J.G. McDaniel, R.G. Holt, Measurement of aqueous foam rheology by acoustic levitation, Phys. Rev. E 61 (2000) R2204–R2207.
[15] S.C. Takatori, R. De Dier, J. Vermant, J.F. Brady, Acoustic trapping of active matter, Nat. Commun. 7 (2016) 10694.
[16] J. Wu, Acoustical tweezers, J. Acoust. Soc. Am. 89 (1991) 2140–2143.
[17] Y. Kenji, U. Shin-ichiro, T. Kazuo, Concentration and fractionation of small particles in liquid by ultrasound, Jpn. J. Appl. Phys. 34 (1995) 2715.
[18] E. van West, A. Yamamoto, T. Higuchi, The concept of "Haptic Tweezer", a non-contact object handling system using levitation techniques and haptics, Mechatronics 17 (2007) 345–356.
[19] Y. Yamakoshi, Y. Noguchi, Micro particle trapping by opposite phases ultrasonic travelling waves, Ultrasonics 36 (1998) 873–878.
[20] V. Vandaele, P. Lambert, A. Delchambre, Non-contact handling in microassembly: acoustical levitation, Precis. Eng. 29 (2005) 491–505.
[21] A. Haake, J. Dual, Positioning of small particles by an ultrasound field excited by surface waves, Ultrasonics 42 (2004) 75–80.
[22] Y. Liu, J. Hu, Trapping of particles by the leakage of a standing wave ultrasonic field, J. Appl. Phys. 106 (2009) 034903.
[23] A. Nilsson, F. Petersson, H. Jönsson, T. Laurell, Acoustic control of suspended particles in micro fluidic chips, Lab Chip 4 (2004) 131–135.
[24] G.R. Goddard, C.K. Sanders, J.C. Martin, G. Kaduchak, S.W. Graves, Analytical performance of an ultrasonic particle focusing flow cytometer, Anal. Chem. 79 (2007) 8740–8746.
[25] F. Petersson, A. Nilsson, C. Holm, H. Jönsson, T. Laurell, Continuous separation of lipid particles from erythrocytes by means of laminar flow and acoustic standing wave forces, Lab Chip 5 (2005) 20–22.
[26] T. Laurell, F. Petersson, A. Nilsson, Chip integrated strategies for acoustic separation and manipulation of cells and particles, Chem. Soc. Rev. 36 (2007) 492–506.
[27] J. Shi, X. Mao, D. Ahmed, A. Colletti, T.J. Huang, Focusing microparticles in a microfluidic channel with standing surface acoustic waves (SSAW), Lab Chip 8 (2008) 221–223.
[28] J. Shi, S. Yazdi, S.-C.S. Lin, X. Ding, I.-K. Chiang, K. Sharp, et al., Three-dimensional continuous particle focusing in a microfluidic channel via standing surface acoustic waves (SSAW), Lab Chip 11 (2011) 2319–2324.
[29] S. Chu, Laser manipulation of atoms and particles, Science 253 (1991) 861–866.
[30] D.G. Grier, A revolution in optical manipulation, Nature 424 (2003) 810–816.
[31] J.P. Barton, D.R. Alexander, S.A. Schaub, Theoretical determination of net radiation force and torque for a spherical particle illuminated by a focused laser beam, J. Appl. Phys. 66 (1989) 4594–4602.
[32] F.M. Moesner, T. Higuchi, Electrostatic devices for particle microhandling, IEEE Trans. Ind. Appl. 35 (1999) 530–536.
[33] M. Washizu, O. Kurosawa, Electrostatic manipulation of DNA in microfabricated structures, IEEE Trans. Ind. Appl. 26 (1990) 1165–1172.
[34] C. Simonnet, A. Groisman, Two-dimensional hydrodynamic focusing in a simple microfluidic device, Appl. Phys. Lett. 87 (2005) 114104.
[35] R. Yang, D.L. Feeback, W. Wang, Microfabrication and test of a three-dimensional polymer hydro-focusing unit for flow cytometry applications, Sens. Actuators, A 118 (2005) 259–267.
[36] C.-C. Chang, Z.-X. Huang, R.-J. Yang, Three-dimensional hydrodynamic focusing in two-layer polydimethylsiloxane (PDMS) microchannels, J. Micromech. Microeng. 17 (2007) 1479.
[37] S. Eyal, S.R. Quake, Velocity-independent microfluidic flow cytometry, Electrophoresis 23 (2002) 2653–2657.
[38] M. Azarpeyvand, Acoustic radiation force of a Bessel beam on a porous sphere, J. Acoust. Soc. Am. 131 (2012) 4337–4348.
[39] M. Azarpeyvand, M. Azarpeyvand, Application of acoustic Bessel beams for handling of hollow porous spheres, Ultrasound Med. Biol. 40 (2014/02/01/ 2014.) 422–433.
[40] L. Zhang, P.L. Marston, Axial radiation force exerted by general non-diffracting beams, J. Acoust. Soc. Am. 131 (2012) EL329–EL335.
[41] P.L. Marston, Axial radiation force of a Bessel beam on a sphere and direction reversal of the force, J. Acoust. Soc. Am. 120 (2006) 3518–3524.
[42] F.G. Mitri, Negative axial radiation force on a fluid and elastic spheres illuminated by a high-order Bessel beam of progressive waves, J. Phys. A: Math. Theor. 42 (2009) 245202.
[43] P.L. Marston, Negative axial radiation forces on solid spheres and shells in a Bessel beam, J. Acoust. Soc. Am. 122 (2007) 3162–3165.
[44] A.L. Bernassau, P.G.A. MacPherson, J. Beeley, B.W. Drinkwater, D.R.S. Cumming, Patterning of microspheres and microbubbles in an acoustic tweezers, Biomed. Microdev. 15 (2013) 289–297.
[45] P.L. Marston, Radiation force of a helicoidal Bessel beam on a sphere, J. Acoust. Soc. Am. 125 (2009) 3539–3547.
[46] X. Chen, R.E. Apfel, Radiation force on a spherical object in the field of a focused cylindrical transducer, J. Acoust. Soc. Am. 101 (1997) 2443–2447.
[47] F.G. Mitri, Theoretical and experimental determination of the acoustic radiation force acting on an elastic cylinder in a plane progressive wave—far-field derivation approach, New J. Phys. 8 (2006) 138.
[48] E.H. Brandt, Acoustic physics: suspended by sound, Nature 413 (2001) 474–475.
[49] C.R.P. Courtney, C.K. Ong, B.W. Drinkwater, A.L. Bernassau, P.D. Wilcox, D.R.S. Cumming, Manipulation of particles in two dimensions using phase controllable ultrasonic standing waves, Proc. Roy. Soc. A: Math., Phys. Eng. Sci. (2011).
[50] J. Lee, K.K. Shung, Effect of ultrasonic attenuation on the feasibility of acoustic tweezers, Ultrasound Med. Biol. 32 (2006) 1575–1583 2006/10/01.
[51] S. Xu, C. Qiu, Z. Liu, Transversally stable acoustic pulling force produced by two crossed plane waves, EPL (Europhys. Lett.) 99 (2012) 44003.
[52] M. Rajabi, A. Mojahed, Acoustic manipulation of a liquid-filled spherical shell activated with an internal spherical oscillator, Acta Acust. United Acust. 103 (2017) 210–218.
[53] M. Azarpeyvand, M. Azarpeyvand, Acoustic radiation force on a rigid cylinder in a focused Gaussian beam, J. Sound Vib. 332 (2013) 2338–2349 2013/04/29.
[54] D. Baresch, J.-L. Thomas, R. Marchiano, Observation of a single-beam gradient force acoustical trap for elastic particles: acoustical tweezers, Phys. Rev. Lett. 116 (2016) 024301.
[55] P.L. Marston, Quasi-Gaussian Bessel-beam superposition: application to the scattering of focused waves by spheres, J. Acoust. Soc. Am. 129 (2011) 1773–1782.
[56] D. Baresch, J.-L. Thomas, R. Marchiano, Three-dimensional acoustic radiation force on an arbitrarily located elastic sphere, J. Acoust. Soc. Am. 133 (2013) 25–36.
[57] A.D. Pierce, Acoustics: An Introduction to its Physical Principles and Applications, Acoustical Society of America Melville, NY, 1991.
[58] M. Abramowitz, I.A. Stegun, Handbook of Mathematical Functions (Applied Mathematics Series 55), National Bureau of Standards, Washington, 1964.
[59] G.T. Silva, An expression for the radiation force exerted by an acoustic beam with arbitrary wavefront (L), J. Acoust. Soc. Am. 130 (2011) 3541–3544.
[60] M.R. Maxey, J.J. Riley, Equation of motion for a small rigid sphere in a nonuniform flow, Phys. Fluids 26 (1983) 883–889.
[61] A. Ardekani, R. Rangel, Unsteady motion of two solid spheres in Stokes flow, Phys. Fluids 18 (2006) 103306.
[62] P.M. Lovalenti, J.F. Brady, The hydrodynamic force on a rigid particle undergoing arbitrary time-dependent motion at small Reynolds number, J. Fluid Mech. 256 (1993) 561–605.
[63] A.A. Doinikov, Acoustic radiation pressure on a rigid sphere in a viscous fluid, Proc. Roy. Soc. London. Ser. A: Math. Phys. Sci. 447 (1994) 447.
[64] A.A. Doinikov, Theory of acoustic radiation pressure for actual fluids, Phys. Rev. E 54 (1996) 6297–6303.
[65] A.A. Doinikov, Acoustic radiation force on a spherical particle in a viscous heat-conducting fluid. I. General formula, J. Acoust. Soc. Am. 101 (1997) 713–721.
[66] A.A. Doinikov, Acoustic radiation force on a spherical particle in a viscous heat-conducting fluid. II. Force on a rigid sphere, J. Acoust. Soc. Am. 101 (1997) 722–730.
[67] A.A. Doinikov, Acoustic radiation force on a spherical particle in a viscous heat-conducting fluid. III. Force on a liquid drop, J. Acoust. Soc. Am. 101 (1997) 731–740.
[68] T. Hasegawa, M. Ochi, K. Matsuzawa, Acoustic radiation force on a solid elastic sphere in a spherical wave field, J. Acoust. Soc. Am. 69 (1981) 937–942.
[69] P. Augustsson, R. Barnkob, S.T. Wereley, H. Bruus, T. Laurell, Automated and temperature-controlled micro-PIV measurements enabling long-term-stable microchannel acoustophoresis characterization, Lab Chip 11 (2011) 4152–4164.
[70] H. Bruus, Acoustofluidics 7: the acoustic radiation force on small particles, Lab Chip 12 (2012) 1014–1021.
[71] X. Ding, Z. Peng, S.-C.S. Lin, M. Geri, S. Li, P. Li, et al., Cell separation using tilted-angle standing surface acoustic waves, Proc. Natl. Acad. Sci. 111 (2014) 12992–12997.
[72] T.F.W. Embleton, The radiation force on a spherical obstacle in a cylindrical sound field, Can. J. Phys. 34 (1956) 276–287.